




# Optical spectroscopy, thermal analysis, and dynamic mechanical properties of graphene nano-platelets reinforced polyvinylchloride

R. M. Ahmed<sup>1,\*</sup> , M. M. Atta<sup>2</sup>, and E. O. Taha<sup>3</sup>

<sup>1</sup> Physics Department, Faculty of Science, Zagazig University, Zagazig 44519, Egypt

<sup>2</sup> Radiation Physics Department, National Center for Radiation Research and Technology (NCRRT), Egyptian Atomic Energy Authority, Cairo, Egypt

<sup>3</sup> Petroleum Applications Department, Egyptian Petroleum Research Institute (EPRI), Cairo, Egypt

Received: 13 June 2021

Accepted: 3 August 2021

Published online:  
12 August 2021

© The Author(s), under exclusive licence to Springer Science+Business Media, LLC, part of Springer Nature 2021

## ABSTRACT

Nanocomposites of graphene nano-platelets (GnPs) with different ratios were embedded in polyvinyl chloride (PVC) by a simple casting technique. DSC and TGA analysis proved that PVC/GnPs (0.5 wt% of GnPs) showed the highest thermal stability. The effects of GnPs on PVC were discussed through studying some important optical parameters besides the thermal properties. Increasing GnPs content increased the thermal stability of the nanocomposites as the residue increased from 1.9% for PVC to 9.3% upon addition of 0.5 wt% of GnPs. The penetration depth ( $\delta$ ), the steepness parameter (S) and the group velocity dispersion (GVD) decreased as the content of GnPs increased. Solar skin protection factor (SSPF) of PVC/GnPs (2.5 wt% of GnPs) nanocomposite improved to be 95% compared with 26% for pure PVC. The optical oscillator strengths ( $f$ ) increased from  $7.97 \text{ (eV)}^2$  for PVC to  $90.8 \text{ (eV)}^2$  for PVC/GnPs (2.5 wt%). The dispersion energy  $E_d$ , the single oscillator energy  $E_o$ , the static refractive index ( $n_o$ ), the oscillator length strength ( $S_o$ ), the average interband oscillator wavelength ( $\lambda_o$ ) were GnPs content dependent. The enhancement in the optical ( $\sigma_{\text{optical}}$ ) conductivity, by increasing the content of GnPs is due to increasing the absorbance of the nanocomposite films. DMA results showed that the storage modulus was increased by 21% upon addition of 0.25 wt% of GnPs while decreased by  $\sim 31\%$  upon increasing GnPs ratio up to 2.5 wt%.

Address correspondence to E-mail: rania.7.8.2016@gmail.com; rmkhalil@zu.edu.eg

## 1 Introduction

Polymer nanocomposites have received much consideration owing to their advantages as easy processing and greater electrical, mechanical, dielectric, and optical properties. Poly (vinyl chloride) (PVC) is one of the most common polymers in the world due to its easy processability, low cost, availability, excellent chemical properties [1–3]. PVC is commercially applied in many applications such as doors, windows, and packaging. By addition plasticizers to PVC, it can be used in the industrial world such as canvas making and plumbing [4]. However, PVC suffers from poor mechanical properties, low thermal stability, and inherent rigidity which limit its contribution in many applications [5].

Thus, different nanofillers were used to tuning PVC properties such as  $\text{WO}_3$  [6], NiO [7], and  $\text{TiO}_2$  [8]. Carbon allotropes such as graphene, reduced graphene oxide, fullerene, and carbon nanotubes were used to improve the mechanical, thermal, optical, and electrical properties of polymeric matrices [9–12]. Graphene with a 2D honeycomb configuration has amazing features as optimum transparency, admirable electronic and mechanical properties [13, 14]. Graphene nanoplatelets (GNPs) are one of the most common graphene phases which have a lamellar structure of multiple ultra-thin graphene lamella [15]. The low-cost mass production of GNPs made it an alternative cheap product to graphene [16]. The integration of GNPs into conventional polymer matrices improves their properties. Therefore, GNPs are widely used in industrial polymers owing to their high mechanical strength (20 GPa) [17]. Also, GNPs have been used to enhance the electromagnetic interference (EMI) shielding effectiveness of PVC and polyaniline composites [18]. The mechanical properties and shape memory of polyurethane were improved upon the addition of GNPs [19]. It was reported that the addition of 0.5 wt% of GNPs produced an obvious enhancement in the tensile strength by 58% and micro hardness by 82 compared with neat PVC [20]. Furthermore, the young's modulus and tensile strength of pure PVC improved by 109%, and 100% respectively, upon addition of 2.5 wt% of GNPs, as published in previous work [1]. Moreover, the optical properties of polymers are important to study the electronic transition and the possibility of their applicability in optical filters such as selection surfaces and greenhouse [21]. The study

of optical absorption spectra of matter provides basic information about the band structure and the energy gap in solids. The optical properties of polymer nanocomposites may be changed upon the addition of various nanoparticles. Deshmukh et al. [22] investigated an improvement in the refractive index and optical conductivity of PVC film with increasing ZnO content. Furthermore, it was reported that doping PVC with 0, 2, 4, and 6 wt%  $\text{Al}_2\text{O}_3$  resulted in decreasing the direct optical energy gap 5.05 to 3.60 eV whereas the Urbach energy increased [23]. Ahmed [21] succeeded in obtaining the dispersion component of surface-free energies of CdSe/ZnS/PVC nanocomposites from the contact angles measurement of only polar liquids by using the surface polarizability hypothesis. The additions of GNPs up to 2.5 wt% were homogeneously distributed in PVC matrix. Moreover, PVC exhibited an improvement of mechanical and dielectric properties as reported in our previous work [1].

As per our knowledge, most of the published papers regarding GNPs -PVC nanocomposites lag behind the study of some important optical parameters as solar material protection factors, optical conductivity ( $\sigma$ ), optical dielectric constants, energy loss function, group velocity dispersion, and dispersion coefficient. Motivated with this, in the present work aforementioned optical parameters of these nanocomposites will be studied in detail. In addition, the thermal and dynamic-mechanical properties of nanocomposite will be investigated.

## 2 Experimental techniques

### 2.1 Materials

From sigma Aldrich Co. USA, PVC and Tetrahydrofuran (THF) solvent were obtained. However, from XG Sciences, Lansing, Michigan, USA, GNPs-grade M was obtained with an average thickness of 6–8 nm and a surface area of 120–150  $\text{m}^2/\text{g}$ .

### 2.2 Preparation of PVC/GNPs composites

A simple casting method was used to prepare films of PVC/GNPs nanocomposites. THF was effectively used to dissolve both of PVC and GNPs. Under sonication for 60 min and stirring for 3 days, the mixtures were kept followed by pouring into Petri

dishes. At room temperature, the prepared samples were dried for 7 days. The films had a thickness of  $\sim 0.28 \pm 0.007$  mm. The nanocomposite films included variant concentrations of GnPs such as (0, 0.25, 0.50, and 2.5 wt%), which are hereafter called C0, C1, C2, and C3, respectively. The concentrations of GnPs were investigated by using the following equation:

$$C(\text{wt}\%) = \frac{W_q \times 100}{W_q + W_p}, \quad (1)$$

where,  $W_q$  and  $W_p$  are the weight of GnPs and PVC, respectively.

### 2.3 Characterization techniques

Mettler Toledo TA-TGA and DSC were used for measuring the thermal stability. The samples were heated in  $N_2$  atm. till  $700^\circ\text{C}$  with a heating rate of  $15^\circ\text{C}/\text{min}$ . The absorption and the specular reflection spectra were recorded with UV-Vis-NIR spectrometer at wavelengths from 190 to 900 nm. DMA was employed to study the thermo-mechanical properties of prepared films of PVC/GnPs nanocomposites. Films were tested utilizing Triton Instruments at different constant frequencies of 0.5, 1, 3 and 5 Hz. The measurements were investigated in the tension mode from room temperature to  $120^\circ\text{C}$  with a heating rate of  $10^\circ\text{C}/\text{min}$ .

## 3 Result and discussion

### 3.1 Thermal analysis

#### 3.1.1 Differential scanning calorimetry (DSC)

The effect of the embedded GnPs on the glass temperature ( $T_g$ ), melting temperature ( $T_m$ ), and melting enthalpy ( $\Delta H_m$ ) of PVC, was studied by DSC analysis. Figure 1 shows the DSC curves of pure PVC and its different PVC/GnPs nanocomposites. The experimentally generated results are summarized in Table 1. The  $T_g$  value of PVC (C0) is  $60.9^\circ\text{C}$  which is so close to some literature data [24]. The observed  $T_g$  value of PVC (C0) is considered to be higher than its nanocomposites (except for C<sub>2</sub>). This behavior affords an easier relaxation of the molecular chain [25]. Also, the higher value of  $T_g$  of PVC than those of nanocomposites of C1 and C2 is due to that H-bonds

of PVC are less strong than the formed H-bonds between it and nanofillers. However, the higher value of  $T_g$  for C2 (0.5 wt% of GnPs), compared to all the other samples is indicative of a restriction in segmental relaxation. The detected result of sample (C2) is consistent with the published literature data [5].

The melting temperatures of PVC (C0) and its nanocomposites, detected from Fig. 1, are listed in Table 1. It can be observed that  $T_m$  of the nanocomposites displays a rising trend by increasing the GnPs content up to C2 then it decreases. The enhancement in the thermal stability of C1 and C2 is due to the homogenous distribution of the nanofiller in PVC, as proved before in a previous study [1], as well as the strong interaction between them [5]. However, the observed decrease in  $T_m$  of C3 (2.5 wt% of GnPs) is attributed to polymer chain restriction caused by excessive GnPs [26].

The enthalpy ( $\Delta H$ ) is considered to be one of the most important thermodynamic properties of materials. The enthalpy can be deduced for a phase transition via integration over its area in the DSC curve [27]. From Table 1, it can be seen that the magnitude of the integrated melting temperature peak provides  $\Delta H_m$  for PVC to be  $0.66$  (J/g) which decreased by increasing GnPs to be  $0.28$  (J/g) for C2 then increased for C3 to become  $0.89$  (J/g).

#### 3.1.2 Thermal gravimetric analysis (TGA)

TGA was employed to examine the thermal stability of PVC and PVC/GnPs nanocomposites. Figure 2 shows the TGA and differential thermogravimetry (DTG) curves of all samples. The obtained thermal parameters are summarized in Table 2. The nanocomposites of C2 and C3 showed three stages of decomposition process compared with four stages for pure PVC (C0) and the nanocomposites C1. For all the tested samples, the first observed decomposition is observed in a range of temperatures from  $160$  to  $200^\circ\text{C}$  (except C1, from  $60$  to  $200^\circ\text{C}$ ), see Fig. 2a, corresponding to DTG peak temperature ( $T1 \approx 186 \pm 10.5^\circ\text{C}$ ), as seen in Fig. 2b and Table 2. This result is ascribed to loss of water from the polymeric chains. The values of T1 decreased by increasing the GnPs content then increased for the highest GnPs content (C3). Decreasing T1 for the nanocomposites of (C1 and C2) compared to PVC C0 is assigned to the assistance of the nanofiller of GnPs in water removing from the polymer structure.

**Fig. 1** DSC curves of PVC (C0 sample) and its nanocomposites (samples of C1, C2, and C3)

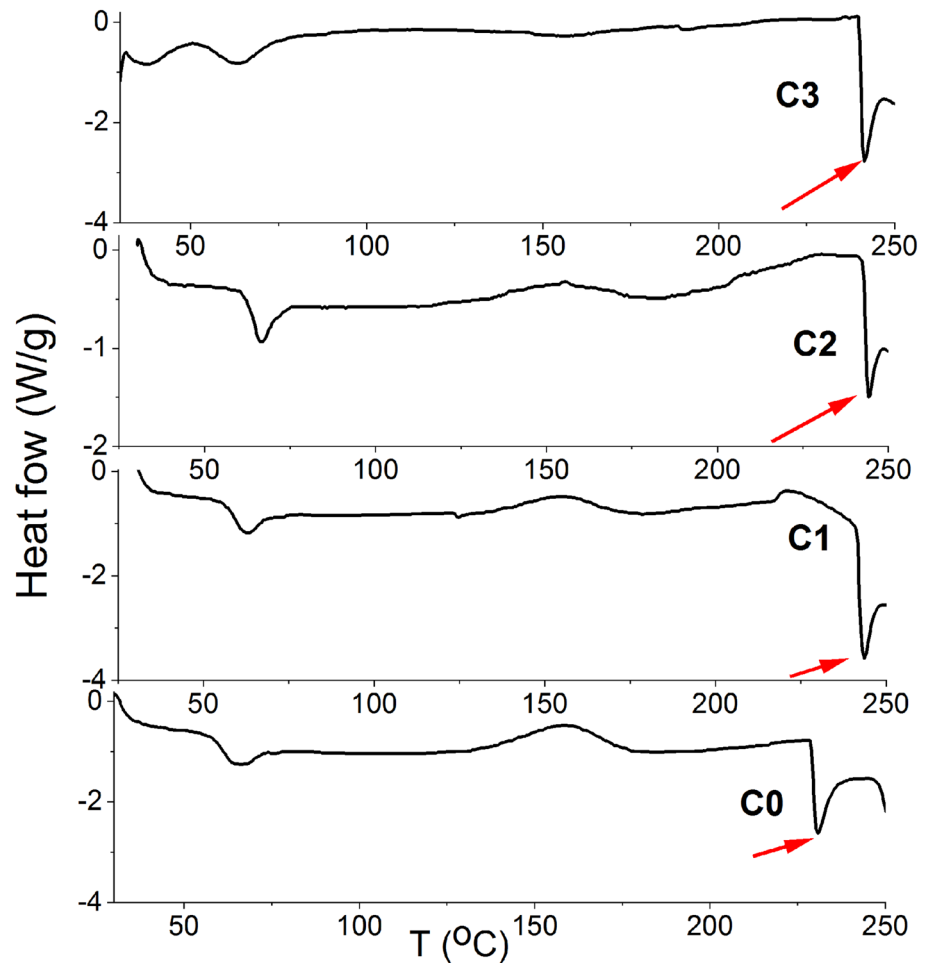


**Table 1** The values of glass transition temperature ( $T_g$ ), melting temperature ( $T_m^P$ ), and melting enthalpy ( $\Delta H_m$ )

| Sample | GnPs (Wt%) | $T_g$ (°C) | $T_m^P$ (°C) | $\Delta H_m$ (J/g) |
|--------|------------|------------|--------------|--------------------|
| C0     | 0          | 60.9       | 230          | 0.66               |
| C1     | 0.25       | 58.9       | 243          | 0.64               |
| C2     | 0.50       | 63.8       | 244          | 0.28               |
| C3     | 2.50       | 58.1       | 241          | 0.89               |

The major degradation of PVC and its nanocomposites is observed in the region from 252 to 386 °C with the corresponding DTG peak temperature ( $T_2 = 292.3 \pm 6.5$  °C), as seen in Table 2. The interpretation of the 2nd stage of decomposition, for PVC and its nanocomposites, as shown in Table 2, is due to release of HCl upon degradation process [5]. In fact, HCl bond is generated from the interaction between Cl radicals originated from C–Cl cleavage

and hydrogen in C–H bonds. The value of  $T_2$  increases as the GnPs content (C1, 0.25 wt% of GnP) and (C2, 0.5 wt% of GnPs) increases in the nanocomposites then it decreases for the highest GnPs content (C3, 2.5 wt%), as seen in Table 2. The observed stability of C1 and C2, in the 2nd stage, can be ascribed to that GnPs have no interaction with atoms of Cl sample which results in strengthen the C–Cl bonds of PVC while this behavior was absent in case of C3 sample [28]. The second stage of decomposition, for all the nanocomposite films, was followed by a thermal stability region between 386 and 443 °C where no weight loss is observed.

Afterward, the third stage of decomposition of PVC/GnPs nanocomposites is occurred from 443 to 525 °C and from 443 to 518 °C for PVC, corresponding to DTGpeak temperature ( $T_3 = 470 \pm 4.99$ ). The 3rd decomposition stage is a result of polyene backbone degradation which causes volatile aromatic complexes creation and a stable residue of the carbonaceous [28]. The values of  $T_3$  for all the

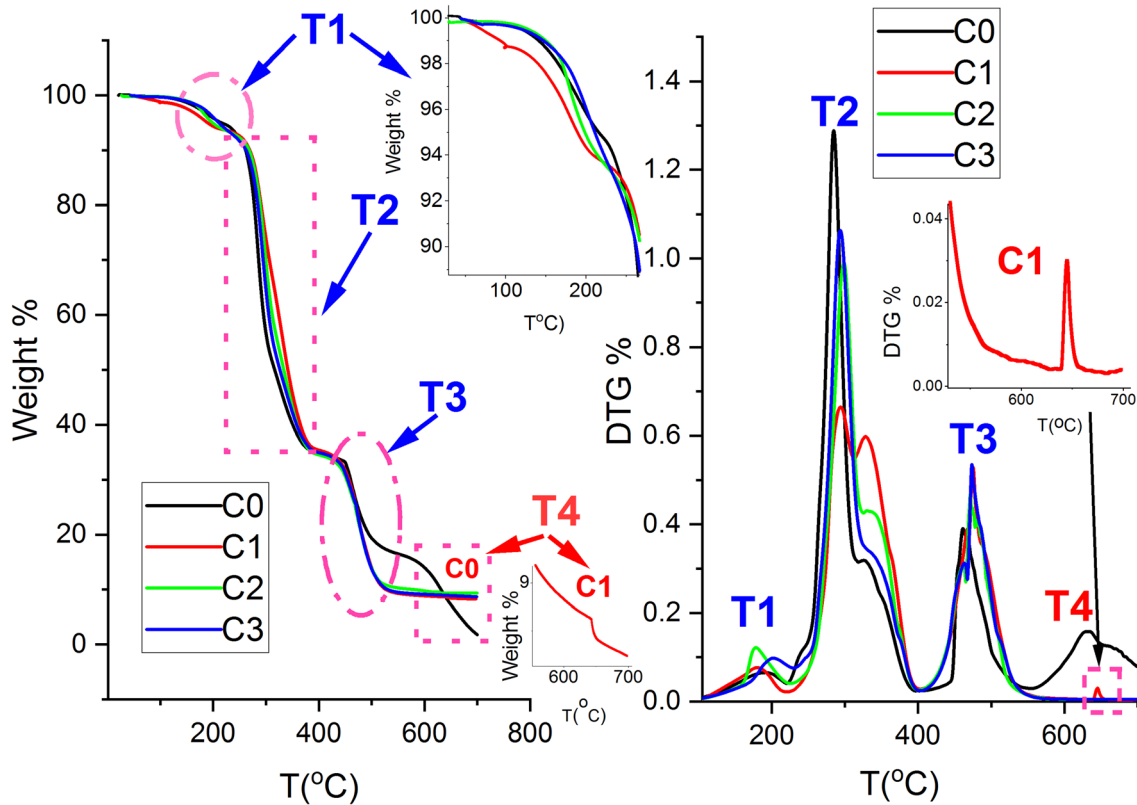


**Fig. 2** Dependence of **a** TGA and **b** DTG % thermograms on temperature for PVC (C0 sample) and its nanocomposites (samples of C1, C2, and C3). The insets are magnification of **a** T1 region and C1 (from 600 to 700 °C) and **b** C1 (from 600 to 700 °C)

**Table 2** TGA thermal parameters for the different PVC/GnPs nanocomposites

| Samples | GnPs (Wt%) | T (°C) range |     |     |     | Weight loss at 700 °C (%) | Residue at 700 °C (%) |
|---------|------------|--------------|-----|-----|-----|---------------------------|-----------------------|
|         |            | T1           | T2  | T3  | T4  |                           |                       |
| C0      | 0          | 195          | 283 | 463 | 632 | 98.1                      | 1.9                   |
| C1      | 0.25       | 178          | 293 | 474 | 646 | 91.5                      | 8.5                   |
| C2      | 0.50       | 177          | 298 | 471 | –   | 90.7                      | 9.3                   |
| C3      | 2.50       | 199          | 295 | 473 | –   | 91.3                      | 8.7                   |

nanocomposites were higher than their hosting matrix of PVC, as observed in Table 2. All the nanocomposites have a thermal stability region from 515 to 700 C followed by their 3rd decomposition (except the decomposition of C1 from 644 to 661 C, the fourth decomposition). However, PVC (C0) has a thermal stability region from 530 to 570 °C then it suffers from decomposition from 570 to 700 °C (the fourth decomposition), as shown in Fig. 2a. The 4th decomposition of pure PVC and C1 existed above ~ 583 °C corresponding to DTG peak temperature of (T4) as observed in Fig. 2b and Table 2. The 4th decomposition of PVC and C1 sample is a result of the reconstruction of the chain structure in

PVC and the nanofillers, in agreement with the literature [29]. At 700 °C, Table 2 provides the percentage of residue (%) of PVC and its nanocomposites. Increasing GnPs content increased the thermal stability of the formed PVC/GnPs nanocomposites as the residue (%) increased from 1.9% for PVC to 9.3% for C2 sample (0.5 wt% of GnPs). Therefore, C2 sample shows the best thermal stability of the fabricated nanocomposites which is in agreement with the DSC results. The enhanced stability of C2 sample can be a result of the strong PVC-GnPs interaction [30].

## 3.2 Optical properties

### 3.2.1 Optical absorbance, transmission, and interband transition

Figure 3a and b illustrate the normalized absorption spectra and transmission spectra, respectively, for PVC/GnPs nanocomposites. The absorption of the host matrix (PVC) enhances by increasing the content of the filler. Also, at 350 nm, the transmission of PVC (C0) decreases from 81.0 to 40.8%, 18.1%, and 5.68% for its nanocomposites of C1, C2, and C3, respectively. The same behavior was observed in a published work [21]. The distance that the electromagnetic wave can be penetrated through the material is known as the penetration depth ( $\delta$ ). The penetration depth is determined in the following manner [31]:

$$\delta(\lambda) = \frac{1}{\alpha}, \quad (2)$$

where  $\alpha$  is the absorption coefficient which is estimated from the following equation [31]:

$$\alpha(\nu) = 2.303 \frac{\text{Absorbance}}{\text{Sample thickness}}. \quad (3)$$

Figure 3c shows the variation of the penetration depth with the wavelength for the different films of PVC/GnPs nanocomposites. The penetration depth increases by increasing the wavelength. Conversely, the penetration depth decreases with increasing the content of GnPs as a result of increasing the absorption possibility of the nanocomposite.

In a previous work [32], it was found that dividing the absorption coefficient ( $\alpha$ ) of the nanocomposite films by that of their host matrix enabled detecting

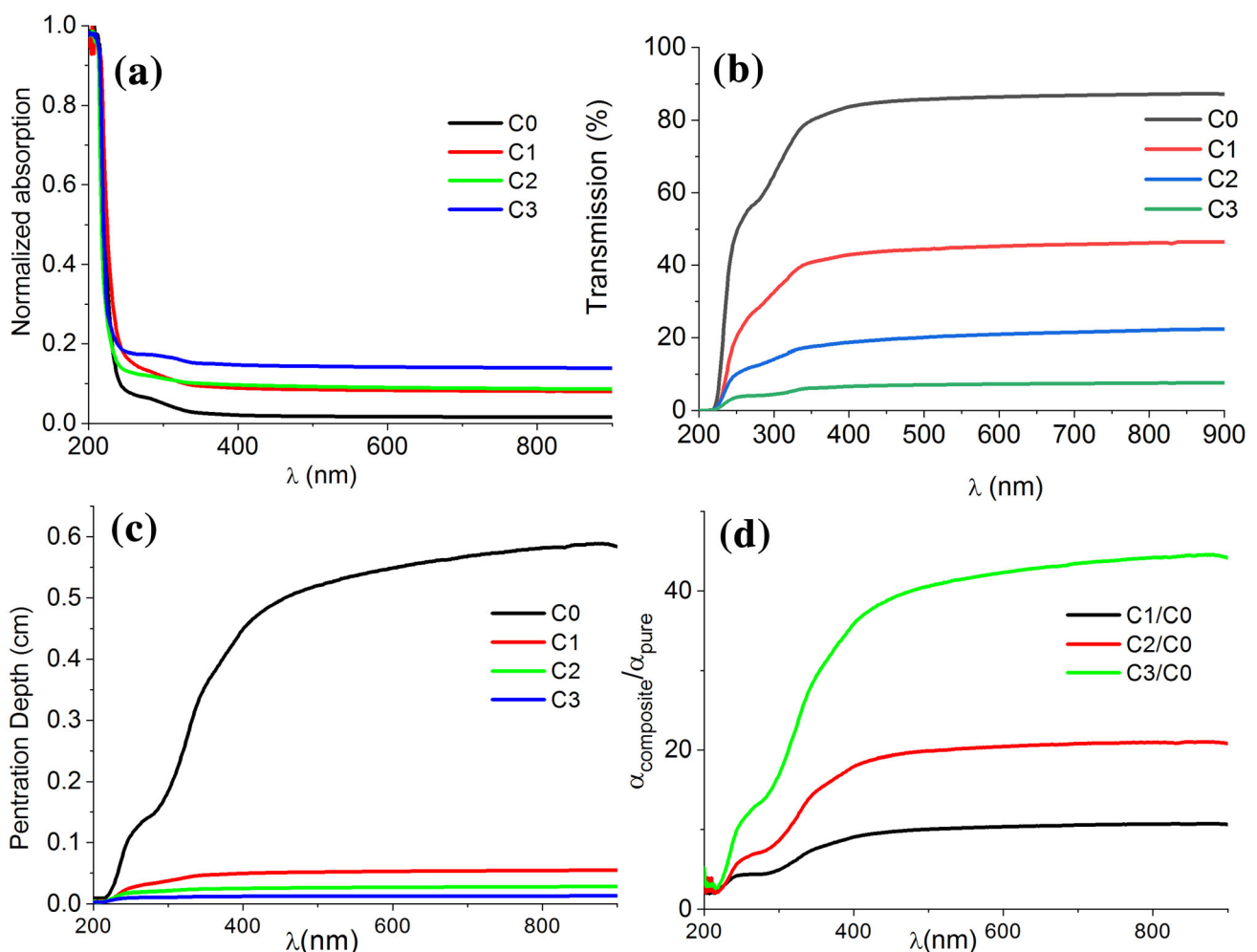


**Fig. 3** Plotting **a** normalized absorption, **b** transmission (%), **c** penetration depth and **d** the absorption coefficient of C1, C2 and C3 divided by the absorption coefficient of PVC versus wavelength for PVC (C0 sample) and its nanocomposites (samples of C1, C2, and C3)

the corresponding absorption peaks of the embedded nanofillers, in the visible region. In case of PVC/GnPs nanocomposites, dividing the absorption coefficient ( $\alpha$ ) of C1, C2, and C3 with C0 showed no absorption peaks for GnPs filler in visible region, see Fig. 3d. This reveals that GnPs have no absorption peak in the visible region.

The absorption coefficient ( $\alpha$ ) shows a steep rise near the absorption edge and a straight line relationship that can be detected in the high  $\alpha$ -region from plotting  $\alpha$ , against the photon energy (E) [32, 33] as shown in Fig. 5a, b for samples of C0 and C3, respectively. The values of the absorption edge,  $A_{edg}$  are deduced from the intercept of the extrapolation to zero absorption in Fig. 5a, b. The tabulated values of  $A_{edg}$  in Table 3 show their dependence on the GnPs content.

The process of transition of electrons between the bands of a solid is defined as the interband absorption process. The band to band transitions are affected by the fundamental absorption. Plotting a graph between  $(\alpha E)^{1/m}$  and (E) is the way to determine the energy of the band gap  $E_g$  by using the following relation [34]:

$$\alpha E = Z(E - E_g)^m \tag{4}$$

where  $z$  is a constant that depends on the transition probability,  $E_g$  is the optical band gap,  $E$  is the photon energy in electron volt. The nature of transition is mainly depending on the value of  $m$  (2, 3, 1/2 and 3/2) which is chosen for the best linear fit for a given data set [34, 35]. By taking natural logarithm and derivation, Eq. (4) can be rewritten as the following:

$$\frac{d \ln(\alpha E)}{dE} = \frac{m}{E - E_g} \tag{5}$$

Figure 4a illustrates a peak in the curve of  $d \ln(\alpha E)/dE$  versus E for C1, as an example for all the samples. This peak is described to be an initial value of gap energy ( $E_{initial}$ ) which is expected to be at energy nearly equals to the optical gap energy ( $E_g$ ). The calculated values of  $E_{initial}$ , are listed in Table 3, which were used, in Fig. 4b, to plot  $\ln(\alpha E)$  versus  $\ln(E - E_g)$  to estimate the proper value of the electronic transition ( $m$ ) from the slope. The value of  $m$ , for all the nanocomposites, was in the order of  $\approx 0.5$ . Therefore, direct allowed transition is supposed to be the predominant transition for all the nanocomposites.

For more accuracy, Eq. (4) was used to determine the optical direct gap energy  $E_{dg}$  by plotting  $(\alpha E)^2$  versus E, see Fig. 5c, d for samples of C0 and C3, as examples for all the samples. The direct allowed transition was investigated from the obtained linear portion in Fig. 5c, d. Therefore, the values of  $E_{dg}$  were deduced from the intercept on the energy axis of the linear fit of the large energy data of the plot. The listed values of  $E_{dg}$ , in Table 3, as well as the values of  $E_{initial}$  decrease by increasing the content of GnPs. These results can be attributed to the defects of GnPs in the bands that lead to the absorption process of the photon energies. The same behavior of the deduced gap energies were previously reported in some literatures [21, 36, 37].

The detected Urbach energy ( $E_u$ ) in disordered and amorphous material acts as a significant parameter which describes their electronic transport properties. The Urbach tails display the defect levels within the forbidden band gap. The absorption process, in this region, can be a result of the transitions between extended states in one band and localized states in the exponential tail of the other band. The empirical formula for deducing Urbach energy is obtained from the following equation [38, 39]

$$\alpha = \alpha_0 \exp\left(\frac{E}{E_u}\right), \tag{6}$$

where  $\alpha_0$  is a constant and  $E_u$  is the Urbach energy that is an indicator of the band tail width of the localized states in the band gap. The values of  $E_u$  were obtained from the reciprocal slope of the linear portion of the plot of  $\ln(\alpha)$  versus energy (E), as seen in Fig. 5e, f for samples of C0 and C3, respectively.

**Table 3** The values of the absorption edge ( $A_{edg}$ ), optical band gaps ( $E_{initial}$  and  $E_{dg}$ ), Urbach energy ( $E_u$ ), the steepness parameter (S), solar material protection factor (SMPF) and solar skin protection factor (SSPF) for PVC (C0 sample) and its nanocomposites (samples of C1, C2, and C3)

| Sample | $E_{initial}$<br>(eV) | $A_{edg}$<br>(eV) | $E_{dg}$<br>(eV) | $E_u$<br>(eV) | S     | SMPF<br>(%) | SSPF<br>(%) |
|--------|-----------------------|-------------------|------------------|---------------|-------|-------------|-------------|
| C0     | 5.46                  | 5.34              | 5.19             | 0.27          | 0.097 | 17          | 26          |
| C1     | 5.45                  | 5.30              | 5.12             | 0.37          | 0.070 | 57          | 63          |
| C2     | 5.44                  | 5.29              | 5.03             | 0.39          | 0.068 | 81          | 84          |
| C3     | 5.41                  | 5.22              | 4.85             | 0.49          | 0.053 | 93          | 95          |

**Fig. 4** Dependence of **a**  $d \ln(\alpha E)/dE$  on  $E$  for all the samples and **b**  $\ln(\alpha E)$  on  $\ln(E - E_{\text{initial}})$  for sample C1

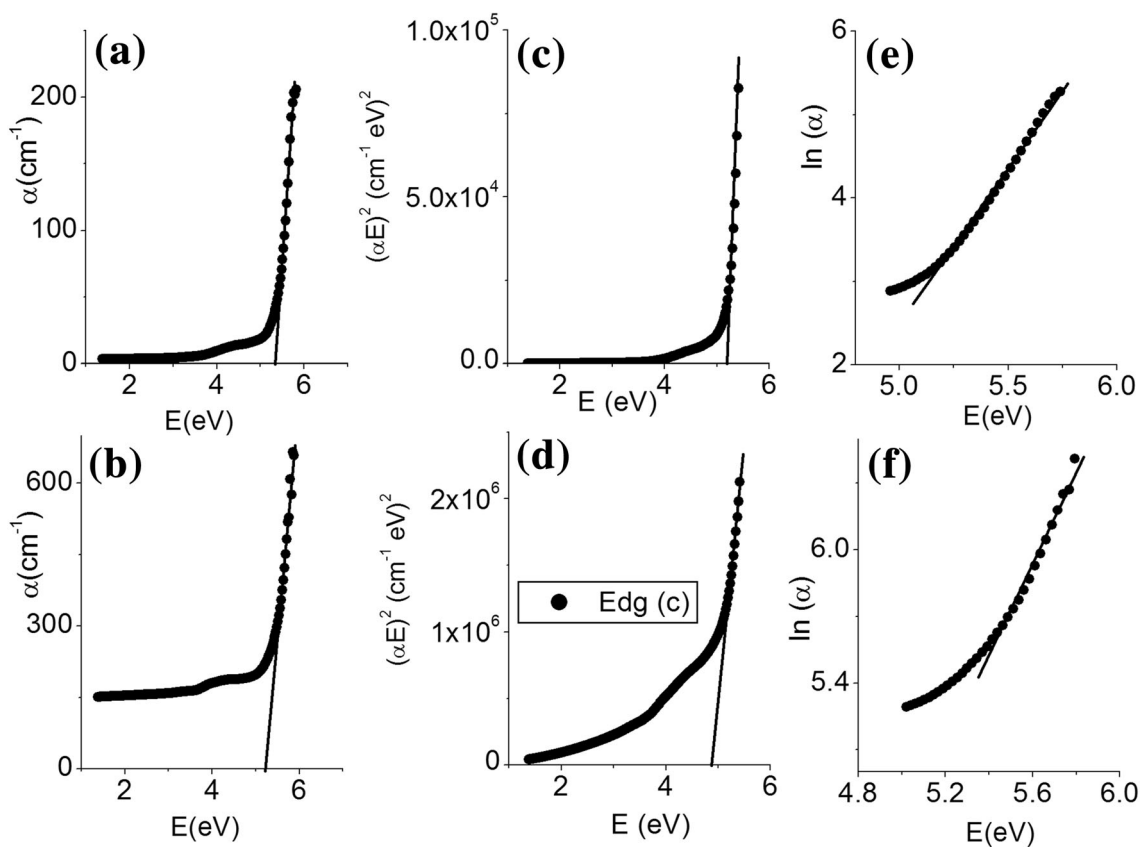
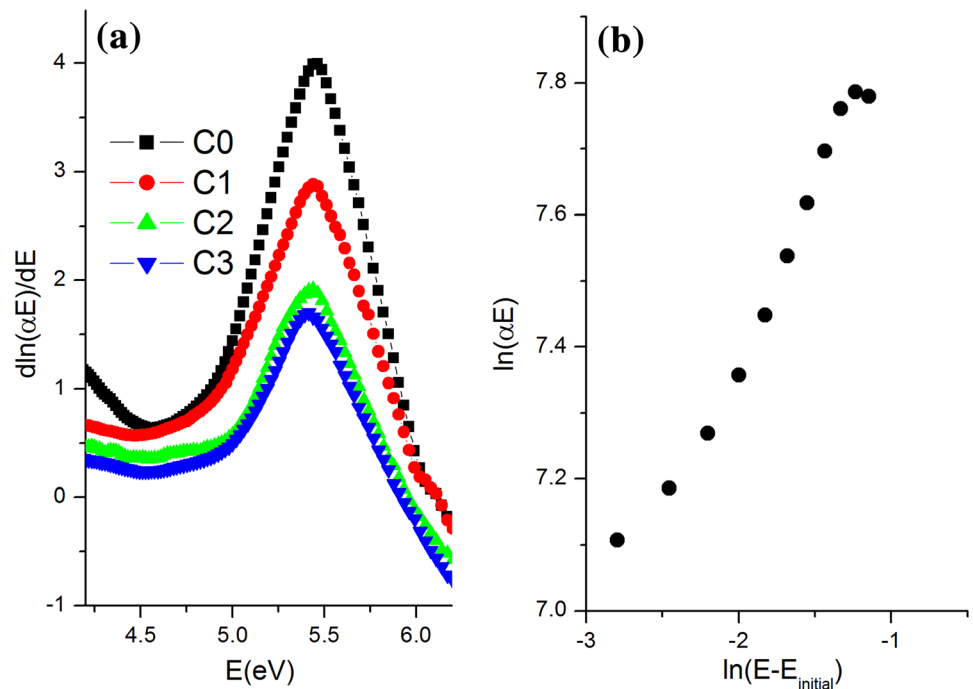


**Fig. 5** Plotting the absorption coefficient ( $\alpha$ ),  $(\alpha E)^2$  and  $\ln(\alpha)$  versus photon energy ( $E$ ) for sample C0 (**a**, **c** and **e**, respectively) and for sample C3 (**b**, **d** and **f**, respectively)



Table 3 shows the increase of  $E_u$  values with increasing the content of GnPs in the nanocomposites. This attitude can be due to increasing the localized state concentration embedded in the band gap [40]. The same behavior was reported in a previous work [21]. The electron–phonon interactions are described by the steepness parameter ( $S$ ) which results in broadening of the absorption edge of PVC/GnPs nanocomposites. The  $S$  values are deduced from the following relation [41]:

$$S = \frac{Tk_B}{E_u}, \tag{7}$$

where  $k_B$  is the Boltzmann constant and  $T$  is the temperature in Kelvin. Increasing disorder in the nanocomposites and formation of localized states in the band gap are the reasons of decreasing the values of  $S$  by increasing the GnPs content as observed in Table 3 [6].

### 3.2.2 Solar protection factors

**3.2.2.1 Solar material protection factor (SMPF)** SMPE is a measure of protection of PVC and its nanocomposites from the degradation produced by solar energy. It can be deduced from the following formula [42]:

$$SMPF = 1 - \left[ \frac{\sum_{\lambda_2}^{\lambda_1} C_\lambda S_\lambda \Delta\lambda T(\lambda)}{\sum_{\lambda_2}^{\lambda_1} C_\lambda S_\lambda \Delta\lambda} \right], \tag{8}$$

where,  $\lambda_1$  equals to 600 nm,  $\lambda_2$  equals to 300 nm,  $S_\lambda$  is the relative spectral distribution of solar radiation [43],  $\lambda$  is the wavelength with nm scale,  $C_\lambda = \exp(-0.012\lambda)$ ,  $T(\lambda)$  is the spectral transmittance of the studied nanocomposites obtained from Fig. 3b,  $\Delta\lambda$  is the wavelength interval ( $\Delta\lambda = 5$  in a range of 300–400 nm and  $\Delta\lambda = 10$  in a range of 400–600 nm),  $C_\lambda S_\lambda \Delta\lambda$  are obtained from a published reference [42].

Table 3 shows that the value of SMPF has increased from 17% of PVC (C0) to 93% for the highest nanocomposite (C3).

**3.2.2.2 Solar skin protection factor (SSPF)** SSPF describes the ability of PVC and its nanocomposites to protect the skin of human beings from destruction caused by solar energy exposure [42].

$$SSPF = 1 - \left[ \frac{\sum_{\lambda_2}^{\lambda_1} E_\lambda S_\lambda \Delta\lambda T(\lambda)}{\sum_{\lambda_2}^{\lambda_1} E_\lambda S_\lambda \Delta\lambda} \right], \tag{9}$$

where  $\lambda_1$  equals to 400 nm,  $\lambda_2$  equals to 300 nm,  $E_\lambda$  is the CIE erythral effectiveness spectrum [43, 44],  $\Delta\lambda$  is the wavelength interval ( $\Delta\lambda = 5$  in  $\lambda$  range from 300 to 400 nm),  $E_\lambda S_\lambda \Delta\lambda$  are given from a published literature [43]. An enhancement in the value of SSPF for C3 sample to be 95% compared with the corresponding value of PVC (C0) which is 26%, as illustrated in Table 3. Consequently, the enhanced values of SMPF and SSPF by increasing the content of GnPs enable using these nanocomposites to reserve effectively materials and human skin from the bad effect of solar energy.

### 3.2.3 Refractive index ( $n$ ) and attenuation coefficient ( $k$ )

Determining the refractive index of polymeric materials is one of their interesting properties because of its significant relation with the local electric field and the electronic polarizability inside the material. Also, the dispersion behavior of the refractive index has an effect on designing optical communication and many optical instruments. Specular reflection ( $R$ ), absorption spectra and therefore the absorption coefficient ( $\alpha$ ) were used to calculate the refractive index ( $n$ ) and the attenuation coefficient ( $k$ ) by using the following relations [45]:

$$n = \left( \frac{1 + R}{1 - R} \right) + \sqrt{\frac{4R}{(1 - R)^2} - k^2} \tag{10}$$

$$k = \frac{\alpha\lambda}{4\pi} \tag{11}$$

The extinction coefficient ( $k$ ) is considered as a measure of the loss in the electromagnetic energy caused by absorption and scattering per unit thickness during its propagation through the material [46]. Figure 6a shows the variation of the extinction coefficient ( $k$ ) with wavelength for PVC (C0) and its nanocomposites. The values of  $k$  increase with increasing the content of GnPs. Also, it increases with increasing the wavelength due to the interaction between the incident light and the polymeric medium [39]. The slow decreasing of the refractive index ( $n$ ) with wavelength provides a typical dispersion curve of the refractive index ( $n$ ) for PVC (C0) and its different nanocomposites, as shown in Fig. 6b. The observed increase in the values of ( $n$ ) with increasing the GnPs content is attributed to formation of intermolecular bonds between PVC and the embedded

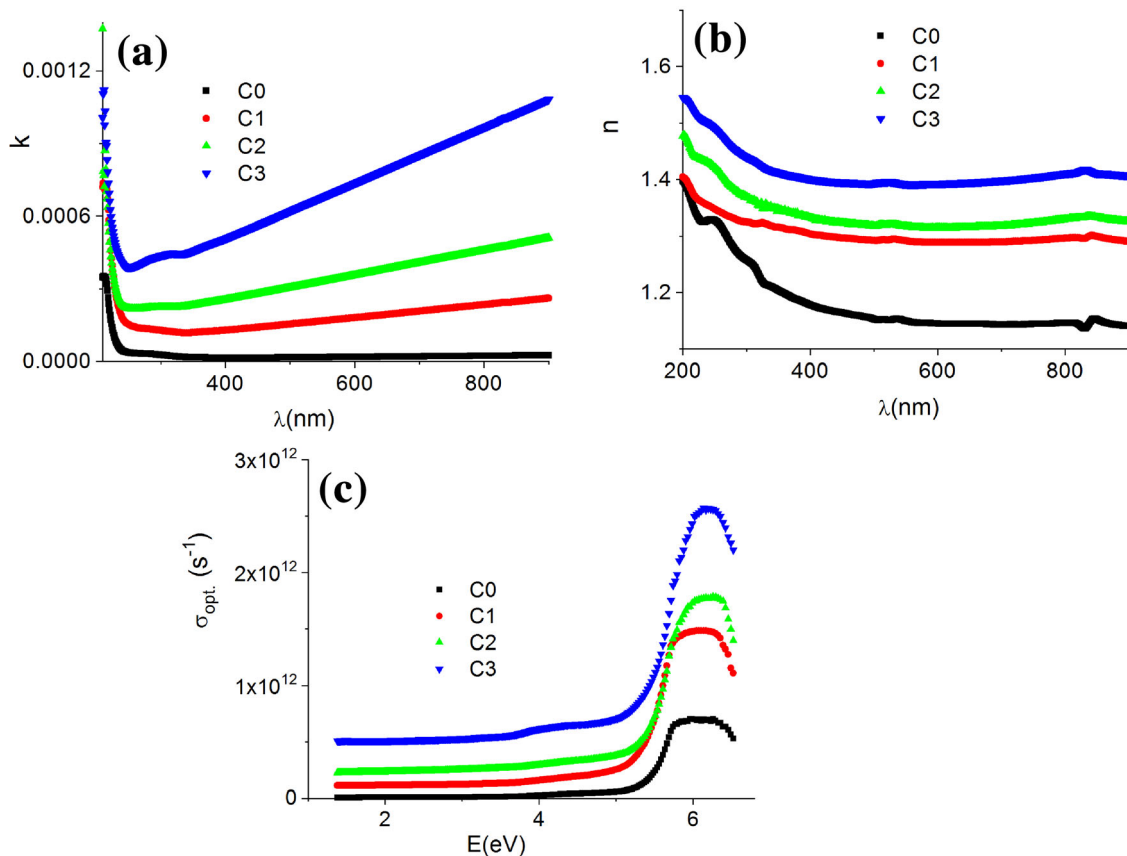


**Fig. 6** Dependence of **a** attenuation coefficient ( $k$ ), **b** refractive index ( $n$ ), and **c** optical conductivity ( $\sigma_{\text{opt}}$ ) on  $E$  for the different nanocomposite films

nanofillers [47]. Such enhancement in the values of  $n$  enables suggesting PVC/GnPs nanocomposites to be applied as antireflection coating for solar cells [47], photonic crystals [48], Bragg gratings [49], and some other optical devices.

### 3.2.4 Optical conductivity ( $\sigma$ )

The velocity of light in space ( $c$ ), the absorption coefficient ( $\alpha$ ) and the refractive index ( $n$ ), were used to calculate the optical conductivity ( $\sigma_{\text{optical}}$ ):

$$\sigma_{\text{optical}} = \frac{cn\alpha}{4\pi} \quad (12)$$

Figure 6c displays the optical conductivity, for PVC (C0) and its variant nanocomposites as functions of the optical energy ( $E$ ). The observed enhancement in the values of the optical conductivity by increasing the content of GnPs is a result of increasing the absorbance of the nanocomposite films [39].

### 3.2.5 Optical dispersion parameters

The theory of the single effective oscillator model proposed by Wemple-DiDomenico (W-D) succeeded in analyzing the dispersion behavior of the refractive index by using the following formula [39, 50]:

$$n^2(E) = 1 + \frac{E_d E_o}{E_o^2 - E^2} \quad (13)$$

where  $E_d$  is the dispersion energy which is a measure of the intensity of the inner band optical transitions and  $E_o$  is the single oscillator energy that is considered as an average gap energy. Plotting  $(n^2 - 1)^{-1}$  versus  $E^2$ , for all the studied films, as seen in Fig. 7a, was used to determine the optical dispersion constants of  $E_d$  and  $E_o$ . Consequently, the intercept on the vertical axis gives  $(E_o/E_d)$  whereas  $(E_o/E_d)^{-1}$  is obtained from the slope. Table 4 shows that  $E_d$  values increase as the GnPs content increases which provides an indication of increasing the bond strength between the nanofiller and host matrix [51]. According to the empirical relation of Tanaka [52], the values

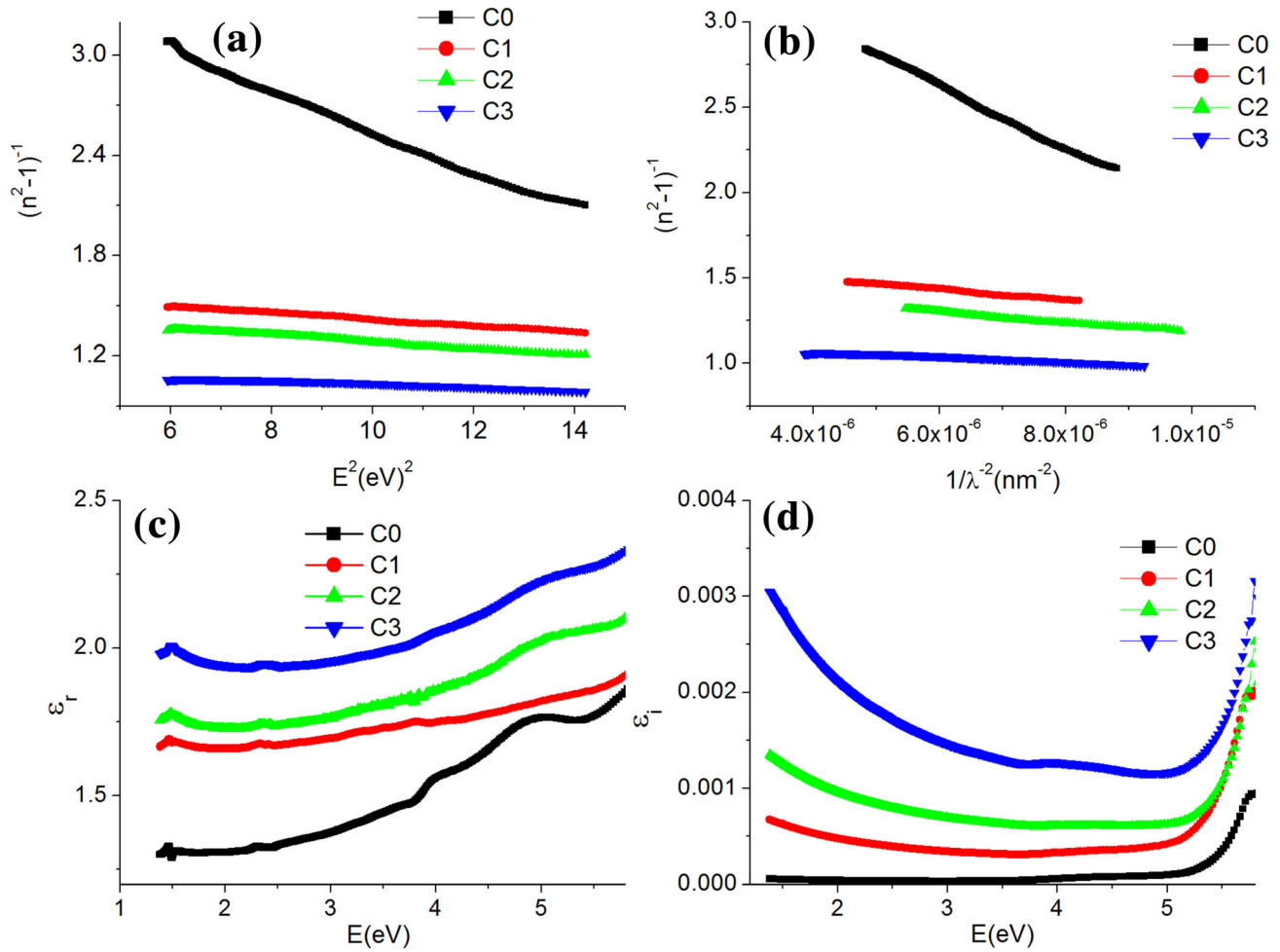


**Fig. 7** For the different nanocomposite films, **a** dependence of  $(n^2 - 1)^{-1}$  on  $E^2$ , **b** dependence of  $(n^2 - 1)^{-1}$  on  $\lambda^2$ , **c** dependence of  $\epsilon_1$  on E, **d** dependence of  $\epsilon_2$  on E

**Table 4** The Wemple-Didomenico oscillating parameters including the values of the dispersion energy  $E_d$ , the single oscillator energy  $E_o$ , the static refractive index ( $n_o$ ), the oscillator strength ( $f$ ), the moments of the optical spectrum ( $M_1$  and  $M_3$ ), the oscillator length strength ( $S_o$ ), and the average interband oscillator wavelength ( $\lambda_o$ ), for PVC (C0 sample) and its nanocomposites (samples of C1, C2, and C3)

| Sample (wt%) | $E_d$ (eV) | $E_o$ (eV) | $n_o$ | $f$ (eV) <sup>2</sup> | $M_1$ | $M_3 \times 10^{-3}$ | $S_o \times 10^{-6}$ (nm) <sup>-2</sup> | $\lambda_o$ (nm) |
|--------------|------------|------------|-------|-----------------------|-------|----------------------|---|------------------|
| C0           | 1.49       | 5.35       | 1.13  | 7.97                  | 0.27  | 8.49                 | 5.22                                    | 223              |
| C1           | 5.64       | 9.10       | 1.27  | 51.3                  | 0.62  | 7.49                 | 31.14                                   | 141              |
| C2           | 5.80       | 8.59       | 1.30  | 49.8                  | 0.67  | 9.16                 | 34.28                                   | 141              |
| C3           | 8.89       | 10.21      | 1.37  | 90.8                  | 0.87  | 8.35                 | 70.87                                   | 112              |

of  $E_o$  are related to the optical energy gap, i.e.  $E_o \approx E_g$  for C0 sample,  $E_o \approx 1.7 E_g$  for C1 and C2 samples and  $E_o \approx 2 E_g$  for C3 sample. The refractive index at zero photon energy is defined as the refractive index dispersion (static refractive index,  $n_o$ ) which was calculated from the following formula [39, 52]:

$$n_o = \sqrt{1 + \frac{E_d}{E_o}} \tag{14}$$

As the content of the nanofiller increases, in PVC/GnPs nanocomposites, the values of  $n_o$  increase as illustrated in Table 4. In addition, the values of  $n_o$

(1.13, 1.27, 1.30 and 1.37 for samples of C0, C1, C2 and C3, respectively), are approximately equal to the corresponding values of the refractive index  $n$ , (1.14, 1.29, 1.32 and 1.40 for samples of C0, C1, C2 and C3, respectively), at long wavelength (900 nm), see Fig. 6b. The absorption of a photon by the electrons between the initial state and the final state is known as the optical oscillator strengths ( $f$ ) which can be computed from the following relation [50, 53]:

$$f = E_o E_d \quad (15)$$

An obvious improvement in the values of optical oscillator strengths ( $f$ ) is observed by increasing GnP's content in the nanocomposites (except C2), as listed in Table 4. The optical spectrum moments ( $M_{-1}$  and  $M_{-3}$ ) are related to the macroscopic quantities such as dielectric constants and the effective number of valence electrons of the material [54]. Also, they describe the inter-band transition strengths which are given from the following equations [55]:

$$E_o^2 = \frac{M_{-1}}{M_{-3}}, \quad (16)$$

$$E_d^2 = \frac{M_{-1}^3}{M_{-3}}, \quad (17)$$

Table 4 shows that by increasing GnP's content in the nanocomposites, the values of  $M_{-1}$  increase whereas the values of  $M_{-3}$  are independent on the filler content. Moss model is used to deduce the average interband oscillator wavelength ( $\lambda_o$ ) and also the oscillator length strength ( $S_o$ ) that describes the strength of the individual dipole oscillator as given by [50, 56]:

$$\frac{(n_\infty^2 - 1)}{(n^2 - 1)} = 1 - \frac{\lambda_o^2}{\lambda^2} \quad (18)$$

Equation (18) can be rewritten to be as the following formula:

$$(n^2 - 1) = \frac{S_o \lambda_o}{1 - (\frac{\lambda_o}{\lambda})^2} \quad (19)$$

The values of  $\lambda_o$  and  $S_o$  were deduced from the slope and intercept of plotting  $(n^2 - 1)^{-1}$  versus  $\lambda^{-2}$  as illustrated in Fig. 7b, for the different nanocomposites. The slope in Fig. 7b gives the quantity of  $1/S_o$ , while the intercept provides the quantity of  $(S_o \lambda_o^2)^{-1}$ . The obtained values of  $S_o$  and  $\lambda_o$ , in Table 4, show

decreasing of  $\lambda_o$  and increasing of  $S_o$  by increasing the nanofiller content.

### 3.2.6 Optical dielectric constants

The real and imaginary parts of the complex dielectric function ( $\epsilon^* = \epsilon_r + i\epsilon_i$ ) are  $\epsilon_r$  and  $\epsilon_i$ , respectively. Interestingly,  $\epsilon_r$  is related to the dispersion which relays on electron motion in the optical medium within the light transmission. However, the dissipative rate of light propagation in the medium is affected by  $\epsilon_i$ . In terms of the refractive index ( $n$ ), and extinction coefficient ( $k$ ), the real and imaginary parts of the optical dielectric constant are obtained from the following relations [57]:

$$\epsilon_r = n^2 - k^2 \quad (20)$$

$$\epsilon_i = 2nk \quad (21)$$

The dependence of  $\epsilon_r$  and  $\epsilon_i$  on the photon energy  $E$ , for all the nanocomposites, is displayed in Fig. 7c, d, respectively. The values of both of  $\epsilon_r$  and  $\epsilon_i$  increase by increasing the GnP's content in the nanocomposites. For all the studied samples, Fig. 7c, d show that, by increasing the photon energy,  $\epsilon_r$  increases with increasing the photon energy while decreases up to  $E \approx 5.1$  eV then it increases. On the other hand, for a highly reflective material, the plasma frequency ( $\omega_p$ ) is calculated by using the real part of optical dielectric constant ( $\epsilon_r$ ) according to the relation [58]:

$$\epsilon_r = \epsilon_\infty - \frac{\omega_p^2}{\omega^2} \quad (22)$$

where  $\epsilon_\infty$  is the dielectric constant at high frequency and  $\omega$  is the angular frequency of the incident light. For PVC and its nanocomposites, a linear relation was obtained, as illustrated in Fig. 8a, from plotting  $\epsilon_r$  versus  $\omega^{-2}$ . In Fig. 8a, the best linear fit provided a slope denotes  $-\omega_p^2$  while the intercept with the axis of  $\epsilon_r$  equals to  $\epsilon_\infty$ . The tabulated values of  $\omega_p$  and  $\epsilon_\infty$ , in Table 5, show that by increasing the content of the nanofiller in the nanocomposites of PVC/GnP's,  $\omega_p$  increases whereas  $\epsilon_\infty$  reduces. Moreover, the plasma frequency ( $\omega_p$ ), can be also calculated by using the following relation [59]:

$$\omega_p^2 = \frac{e^2}{\epsilon_o} \left( \frac{N}{m^*} \right) \quad (23)$$

where  $N$  is that the free charge-carrier concentration,  $m^*$  is the effective mass of the charge carriers (in unit

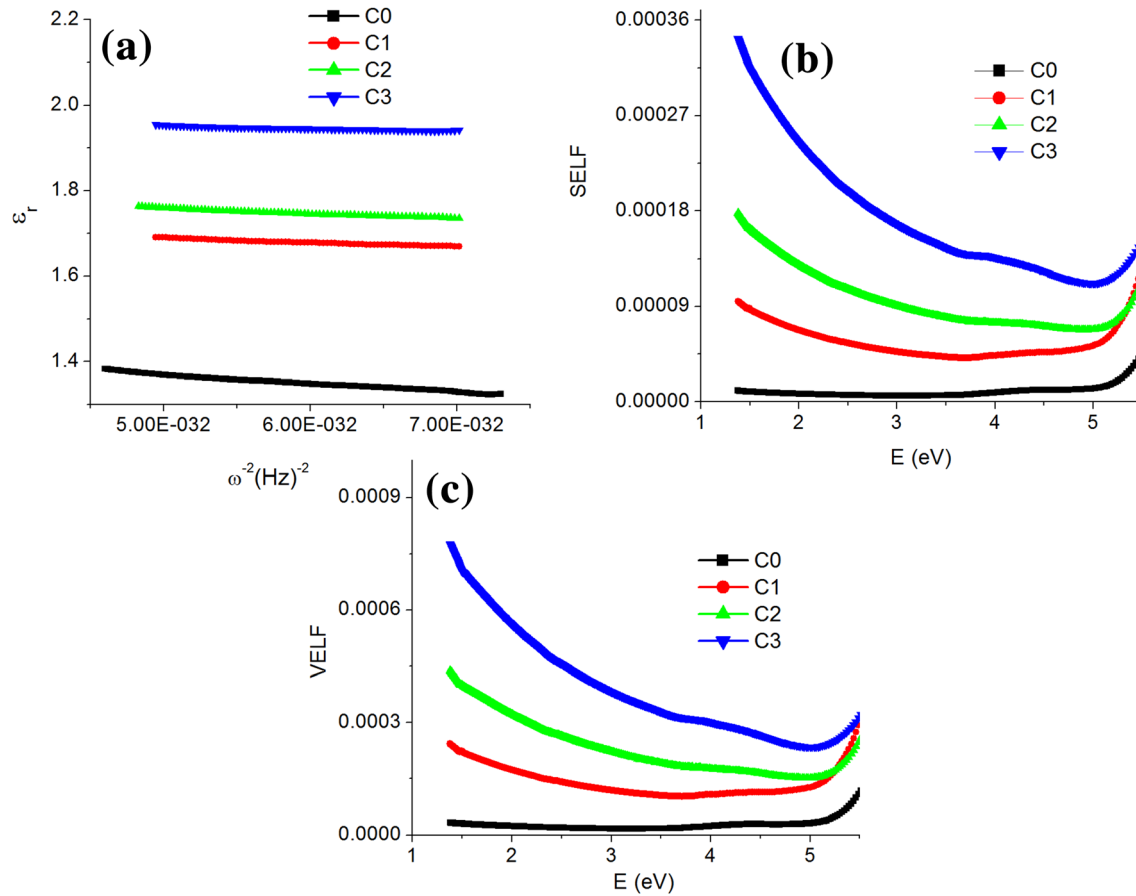


**Fig. 8** For the different nanocomposite films, **a** dependence of  $\epsilon_r$  on  $\omega^{-2}$  and dependence of **b** VELF and **c** SELF on  $E$

**Table 5** The values of plasma frequency ( $\omega_p$ ), the high frequency dielectric constant ( $\epsilon_\infty$ ),  $N/m^*$ , the group velocity dispersion (GVD) and the dispersion coefficient for material dispersion ( $D$ ), for PVC (C0 sample) and its nanocomposites (samples of C1, C2, and C3)

| Sample | $\omega_p \times 10^{15}$<br>(Hz) | $\epsilon_\infty$ | $(N/m^*) \times 10^{57}$<br>$(\text{kg m}^3)^{-1}$ | GVD<br>$(\text{fs}^2/\mu\text{m})$ | $D$ $(\text{fs}^2/\mu\text{m}^2)$ |
|--------|-----------------------------------|-------------------|--|------------------------------------|-----------------------------------|
| C0     | 1.41                              | 1.48              | 1.10   | 352                                | – 963                             |
| C1     | 1.10                              | 1.75              | 0.67   | 142                                | – 389                             |
| C2     | 1.09                              | 1.82              | 0.66   | 24                                 | – 67                              |
| C3     | 0.79                              | 1.98              | 0.35   | 22                                 | – 64                              |

of  $k_g$ ),  $\epsilon_0$  is the permittivity of the free space and  $e$  is that the charge of the electron. The deduced values of  $(N/m^*)$ , from Eq. (23), in Table 5, reduce by increasing the GnPs content in the PVC/GnPs nanocomposites.

### 3.2.7 Energy loss function

The surface energy loss function (SELF) is considered as a measure of the energy loss caused by surface

material penetration. However, the energy loss upon light penetration into a bulk material is described by the volume energy loss function (VELF). The real ( $\epsilon_r$ ) and the imaginary ( $\epsilon_i$ ) parts of the dielectric constant are used to obtain the values of (VELF) and (SELF) as the following [60]:

$$SELF = \frac{\epsilon_i}{(\epsilon_r + 1)^2 + \epsilon_i^2} \tag{24}$$

$$VELF = \frac{\varepsilon_i}{\varepsilon_r^2 + \varepsilon_i^2}. \quad (25)$$

The variation of SELF and VELF with energy for PVC and its nanocomposites are shown in Fig. 8b, c, respectively. A clear enhancement in the values of SELF and VELF is detected by increasing the GnP content in the nanocomposites of PVC/GnPs.

### 3.2.8 Group velocity dispersion (GVD) and dispersion coefficient (D)

The group velocity dispersion (GVD) is associated with the second derivative of refractive index with respect to the wavelength of the incident light. GVD can describe the dispersion of the nanocomposites by using the following relation [61]:

$$GVD = \frac{\lambda^3}{2\pi c^2} \left( \frac{d^2 n}{d\lambda^2} \right) \quad (26)$$

Plotting the 2nd derivative of refractive index versus the incident light wavelength, as shown in Fig. 9, were useful to obtain the values of GVD. Figure 9 displays a short pulse of light which spreads in time as a consequence of variant frequency components of the traveled pulses with diverse velocities. The tabulated values of GVD, in Table 5, illustrate their decreasing by increasing the content of GnPs in the PVC/GnPs nanocomposites. Therefore, PVC/GnPs nanocomposites are not effective for laser pulse broadening. On the other hand, GVD is related to the dispersion coefficient dispersion (D) by the formula of [61]:

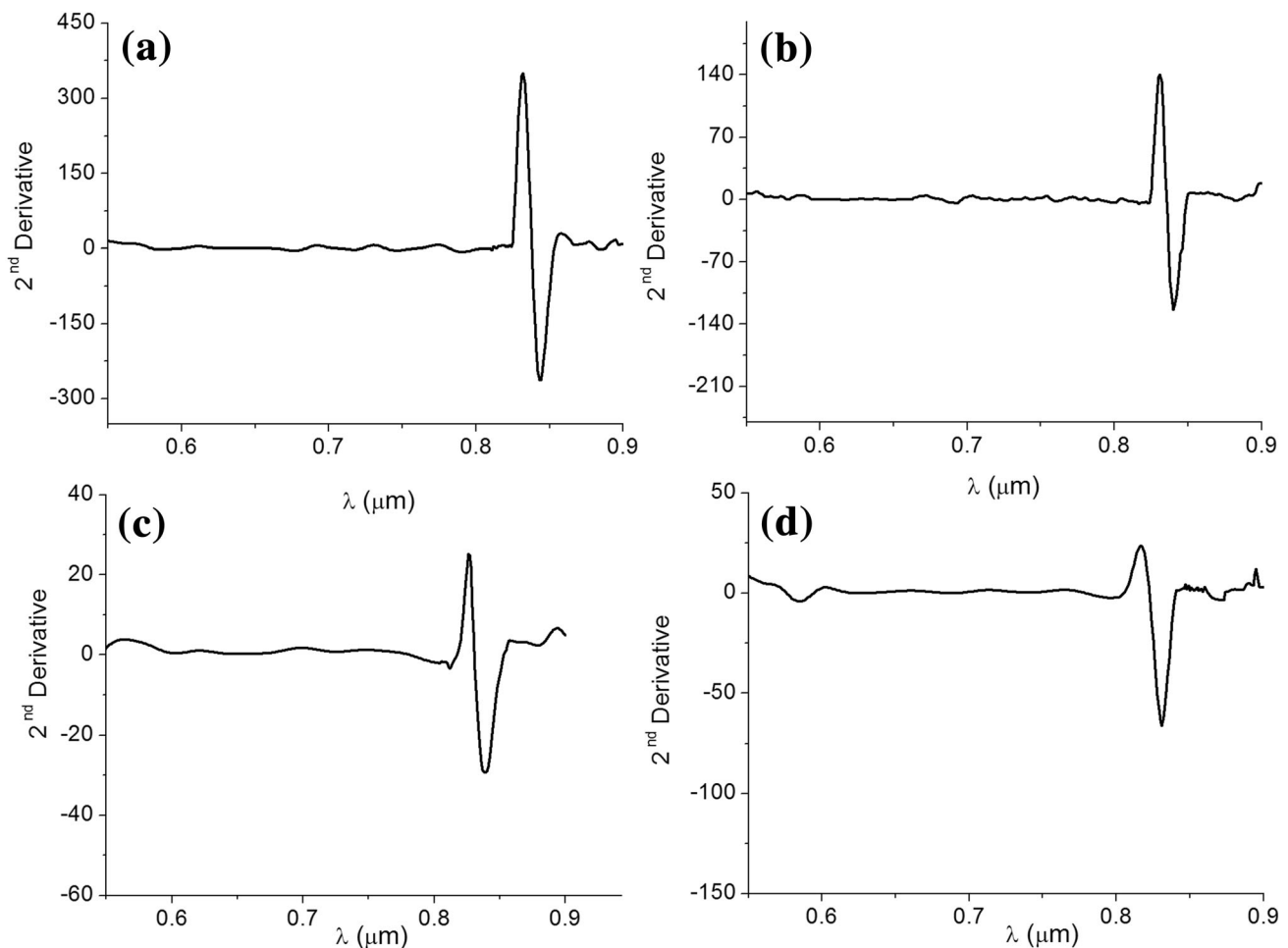


**Fig. 9** Plotting the second derivative of refractive index versus the wavelength for samples of **a** C0, **b** C1, **c** C2 and **d** C3

$$D = -\frac{\lambda}{c} \left( \frac{d^2n}{d\lambda^2} \right) = \frac{-2\pi c}{\lambda^2} GVD \tag{27}$$

Obtaining negative values of  $D$  ( $D < \text{zero}$ ) provides a positive dispersion medium while getting positive value of  $D$  ( $D > \text{zero}$ ) gives negative dispersion medium. The listed negative values of  $D$  in Table 5 confirm that PVC and its nanocomposites have positive dispersion.

### 3.3 Dynamic mechanical properties

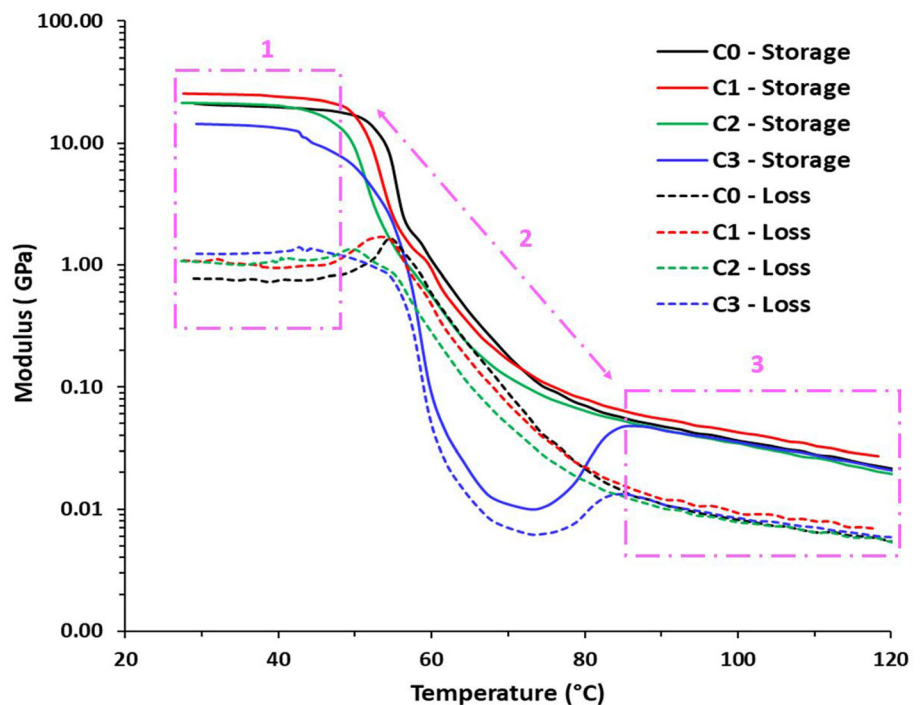
#### 3.3.1 The storage and the loss modulus

The dynamic mechanical analysis (DMA) describes the filler-matrix interactions, the storage modulus curve that reveals the elastic behavior and the loss modulus in which the molecular motion of the polymer matrix can be understood [62].

The storage and the loss modulus, as a function of temperature, at a constant frequency of 1 Hz, for pure PVC (C0) and nanocomposites of PVC/GnPs, are shown in Fig. 10. The storage modulus shows a decreasing trend and goes from glassy state to rubbery state through the glass transition region. In the glassy state (region 1 in Fig. 10), the highest storage modulus is found at C1 nanocomposite then the modulus decreases as GnPs content increases until

reaching the minimum value for sample of C3. The values of storage modulus of pure PVC (C0) and PVC/GnPs nanocomposites (C1, C2 and C3) at 30 °C are 2.08 GPa, 2.51 GPa, 2.12 GPa and 1.43 GPa, respectively. This means that the storage modulus of C1 and C2 nanocomposite increased by about 21% and 2.2%, respectively, compared with C0 (pure PVC). However, the storage modulus of C3 nanocomposite decreases by about 30.9%. Similar results for concentrations of 0.01 wt% and 0.15 wt% of graphene oxide were obtained with graphene/polymer composites [63]. The weakening of the chemical bond between graphene and the polymer material might be a reason for reducing the storage modulus [63]. Another reason is that carbon agglomerations tend to be greater at high carbon concentrations during the composite process and chemical bonds created by the polymer chains are weaker [64]. In the transition state (region 2 in Fig. 10), the storage modulus significantly decreases by three orders of magnitude because the molecules made a shift from a glassy state to a rubbery state in this temperature range. The maximum drop in modulus is found for C3 sample with a minimum drop peak at approximately 70 °C. The same behavior is found with the same drop peak with GnPs/maleated-PLA nanocomposites [65]. In the rubbery state (region 3 in Fig. 10), the small values of

**Fig. 10** Storage and loss modulus as a function of temperature at 1 Hz for PVC/GnPs nanocomposites



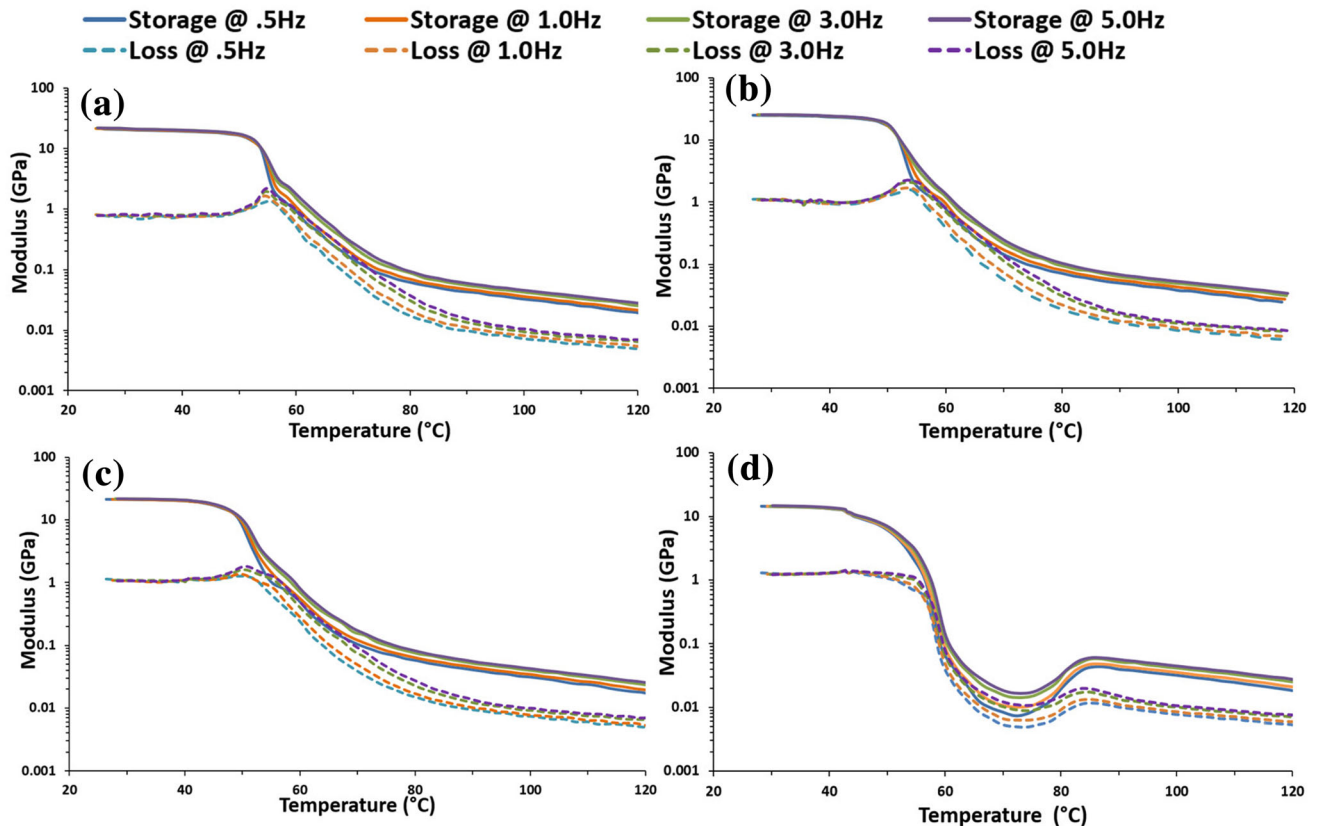


**Fig. 11** Storage and loss modulus, as a function of temperature and at constant frequencies of 0.5, 1, 3, and 5 Hz, for **a** C0, **b** C1, **c** C2, and **d** C3, respectively

**Table 6** The glass transition temperatures ( $T_g$ ) for PVC/GnPs nanocomposites at constant frequencies of 0.5, 1, 3, and 5 Hz

| Samples | GnPs (wt%) | Glass transition temperature ( $T_g$ ) |        |        |        |
|---------|------------|--|--------|--------|--------|
|         |            | 0.5 Hz                                 | 1.0 Hz | 3.0 Hz | 5.0 Hz |
| C0      | 0          | 53.9                                   | 54.5   | 54.7   | 54.8   |
| C1      | 0.25       | 51.5                                   | 52.1   | 52.4   | 55.3   |
| C2      | 0.50       | 49.2                                   | 49.8   | 50.2   | 50.5   |
| C3      | 2.50       | 42.6                                   | 42.7   | 42.8   | 42.8   |

storage module are owing to the energy dissipation involving cooperative motions of the polymer chains [1]. There was no major change in the storage modulus for all nanocomposites except for sample of C1. The higher storage modulus of C1 sample, overall temperature ranges, enables predication of the improved thermal stability compared to other composites which resulted in the potential for higher temperature application.

Figure 8 shows also the loss modulus which quantifies the greatest amount of heat that may be lost every cycle during deformation [66]. The loss modulus exhibited the same trend as storage modulus behavior except at the glassy state where the loss modulus increases with GnPs content. The increased value of the loss modulus is due to a rise in the internal friction, which increases the dissipation energy. The loss modulus curve attained its highest value at the point of maximal mechanical energy dissipation. There is also an apparent shift in the glass transition temperature ( $T_g$ ) (the highest peak in the loss modulus curve) towards the low temperature as the GnPs content increases. The values of  $T_g$  are 54.5 °C, 52.1 °C, 49.8 °C, and 42.7 °C for C0, C1, C2, and C3 nanocomposites, respectively. It is possible to see a difference between the  $T_g$  values acquired using DSC and DMA. This distinction is related to the fact that the DSC and DMA instruments operate in quite different ways [67].



### 3.3.2 The effect of frequency

The variation of the storage and the loss modulus with frequency as a function of the temperature of pure PVC and PVC/GnPs nanocomposites are shown in Fig. 11a–d. The storage and the loss modulus are not affected by frequency at glassy state while they are considerably affected by frequency at both transition and rubbery states. This is due to that, at high temperatures, the filler agglomerates and the linkages between the filler and the polymer matrix generally break down, and that leads to a dramatic shift in modulus values [68]. Furthermore, the storage and the loss modulus demonstrate greater values at higher frequencies in comparison with those at lower frequencies. This characteristic behavior is observed for all the nanocomposites because the time required for oscillation of the molecular chain is considerably shorter than the time for relaxation. Additionally, long-time measurement mode for samples subjected to relentless oscillating forces enables them to be very elastic. Therefore, it can be a significant contributing component to an increase in the storage modulus value [69]. Table 6 represents glass transition temperatures extracted from the loss modulus curves. The  $T_g$  increases with increasing the applied frequencies and decreases with GnPs content. The mechanism of  $T_g$  decrement in polymer composites is more complicated and the value of  $T_g$  is obviously affected by the molecular weight, adhesion factor, and cross-linking density, among other factors [70].

## 4 Conclusions

Different nanocomposites of PVC and GnPs were successfully prepared by the solution casting method. DSC curves showed that the melting enthalpy,  $\Delta H_m$  for PVC is 0.66 (J/g) which decreased to be 0.28 (J/g) for C2 and then increased to be 0.89 (J/g) for C3. The nanocomposites of C2 and C3 showed three stages of decomposition process, in its TGA curves, compared with four stages for pure PVC (C0) and the nanocomposites C1. By increasing the content of GnPs, the values of  $E_{dg}$  and  $E_{initial}$  decreased. These results can be attributed to the defects of GnPs in the bands that lead to the absorption process of the photon energies. Increasing the refractive index by increasing the GnPs content is a result of formation of intermolecular bonds between PVC and the

embedded nanofiller. Such enhancement in the values of  $n$  enables suggesting PVC/GnPs nanocomposites to be applied in different optical devices. The solar material protection factor (SMPF) of PVC increased by increasing the content of GnPs. By increasing the content of the nanofiller in the nanocomposite,  $\omega_p$  increased whereas  $\epsilon_\infty$  reduced. The values of the ratio of  $(N/m^*)$  reduced by increasing the GnPs content. The negative values of dispersion coefficient dispersion (D) confirm that PVC and its nanocomposites have positive dispersion. DMA properties of GnPs nanocomposites were examined and compared. The results showed that the highest storage modulus was found in the C1 nanocomposite overall temperature ranges where the storage modulus increased by 21%. The storage and the loss modulus were found to be greatly affected by frequencies, especially at high-temperature ranges. The glass transition temperature of GnPs nanocomposites was also inferred by DMA. The glass transition temperature decreased as the GnPs contents while it increased with increasing the applied frequencies.

## References

1. R. Ahmed, A. Ibrahim, A. El-Bayoumi, M. Atta, Int. J. Polym. Anal. Charact **26**, 68 (2021)
2. M. Hasanzadeh, M.R. Ghahhari, S.M. Bidoki, J. Mater. Sci.: Mater. Electron. **32**, 15789 (2021)
3. R. Aepuru, V.M. Gaikwad, R. Udayabhaskar, H. Panda, M.R. Viswanathan, J. Mater. Sci.: Mater. Electron. **31**, 13477 (2020)
4. B.-Y. Peng, Z. Chen, J. Chen, H. Yu, X. Zhou, C.S. Criddle, W.-M. Wu, Y. Zhang, Environ. Int. **145**, 106106 (2020)
5. F. Mindivan, M. Göktaş, Polym. Bull. **77**, 1929 (2020)
6. A. Henaish, A. Abouhaswa, Bull. Mater. Sci. **43**, 1 (2020)
7. A. Muzaffar, M.B. Ahamed, K. Deshmukh, M. Faisal, Polym. Test **77**, 105925 (2019)
8. V. Mathur, R. Bremananth, P.K. Arya, Micron **139**, 102952 (2020)
9. D.G. Papageorgiou, I.A. Kinloch, R.J. Young, Prog. Mater. Sci. **90**, 75 (2017)
10. M. Baibarac, L. Stingescu, M. Stroe, C. Negrila, E. Matei, L.C. Cotet, I. Anghel, I.E. Şofran, L. Baia, Polymers **13**, 565 (2021)

11. J. Peng, Y. Wu, W. Ye, D.A. Jacobs, H. Shen, X. Fu, Y. Wan, N. Wu, C. Barugkin, H.T. Nguyen, *Energy Environ. Sci.* **10**, 1792 (2017)
12. Y. Wu, X. Lin, M. Zhang, *J. Nanomater.* **2013**, 627215 (2013)
13. T.A. Amollo, G.T. Mola, V.O. Nyamori, *J. Mater. Sci: Mater. Electron.* **29**, 7820 (2018)
14. M. Atta, M.A. Maksoud, O. Sallam, A. Awed, *J. Mater. Sci.: Mater. Electron.* **32**, 3688 (2021)
15. A. Sadoun, A. Fathy, *Ceram. Int.* **45**, 24784 (2019)
16. Y.-S. Jun, J. Um, G. Jiang, A. Yu, *Express Polym. Lett.* **12**, 885–897 (2018)
17. Y. Zhang, S.F. Ali, E. Dervishi, Y. Xu, Z. Li, D. Casciano, A.S. Biris, *ACS Nano* **4**, 3181–3186 (2010)
18. M.F. Shakir, A.N. Khan, R. Khan, S. Javed, A. Tariq, M. Azeem, A. Riaz, A. Shafqat, H.M. Cheema, M.A. Akram, *Results Phys.* **14**, 102365 (2019)
19. K.K. Patel, R. Purohit, *Sens. Actuator A* **285**, 17 (2019)
20. F. Mindivan, M. Göktaş, A.S. Dike, *Polym. Compos.* **41**, 3707 (2020)
21. R. Ahmed, *Polym. Compos.* **38**, 749 (2017)
22. S. Deshmukh, D. Burghate, S. Shilaskar, G. Chaudhari, P. Deshmukh, *Indian J. Pure Appl. Phys.* **46**, 344–348 (2008)
23. W. Al-Taay, M.A. Nabi, R.M. Yusop, E. Yousif, B.M. Abdullah, J. Salimon, N. Salih, S.I. Zubairi, *Int. J. Polym. Sci.* (2014). <https://doi.org/10.1155/2014/697809>
24. E.V. Belukhichev, V.E. Sitnikova, E.O. Samuylova, M.V. Uspenskaya, D.M. Martynova, *Polymers* **12**, 270 (2020)
25. M. Anggaravidya, E. Budianto, I. Gunawan, *Proced. Chem.* **4**, 107–113 (2012)
26. M. Goumri, C. Poilâne, P. Ruterana, B.B. Doudou, J. Wéry, A. Bakour, M. Baitoul, *Chin. J. Phys.* **55**, 412 (2017)
27. R.M. Ahmed, A. Abd Elbary, *Arab. J. Nucl. Sci. Appl.* **51**, 51 (2018)
28. S. Vadukumpully, J. Paul, N. Mahanta, S. Valiyaveetil, *Carbon* **49**, 198 (2011)
29. Z. Wang, R. Wei, X. Wang, J. He, J. Wang, *Materials* **11**, 1997 (2018)
30. Y. Wu, Q. Liu, Z. Heng, H. Zou, Y. Chen, M. Liang, *Polym. Compos.* **40**, 3866 (2019)
31. R. Ahmed, A. Ibrahim, E. El-Said, *Acta Phys. Polon. A* **137**, 317–323 (2020)
32. R.M. Ahmed, *Arab. J. Nucl. Sci. Appl.* **51**, 9 (2018)
33. A. Alias, N. Sahapini, S. Khalid, Z. Zabidi, *Adv. Mater. Res.* **660**, 15 (2013)
34. R. Ahmed, *Int. J. Polym. Mater.* **57**, 969 (2008)
35. E. Davis, N. Mott, *Philos. Mag.* **22**, 0903 (1970)
36. T. Taha, Z. Ismail, M. Elhawary, *Appl. Phys. A* **124**, 1 (2018)
37. A. El Sayed, W. Morsi, *Polym. Compos.* **34**, 2031 (2013)
38. S.B. Aziz, H.M. Ahmed, A.M. Hussein, A.B. Fathulla, R.M. Wsw, R.T. Hussein, *J. Mater. Sci.: Mater. Electron.* **26**, 8022 (2015)
39. R. Ahmed, A.A. Ibrahim, E.A. El-sayd, *Arab. J. Nucl. Sci. Appl.* **52**, 22 (2019)
40. G. Fanchini, A. Tagliaferro, *Appl. Phys. Lett.* **85**, 730 (2004)
41. V. Raja, A. Sarma, V.N. Rao, *Mater. Lett.* **57**, 4678 (2003)
42. B.P. Jelle, A. Gustavsen, T.N. Nilsen, T. Jacobsen, *Sol. Energy Mater. Sol. Cell* **91**, 342 (2007)
43. ISO, *International Organization for Standardization* (ISO, Geneva, 2003)
44. A. McKinlay, B. Diffey, *CIE J.* **6**, 17 (1987)
45. R. Ahmed, *Int. J. Photoenergy* (2009). <https://doi.org/10.12968/indn.2009.15.5.76672>
46. S.B. Aziz, O.G. Abdullah, A.M. Hussein, R.T. Abdulwahid, M.A. Rasheed, H.M. Ahmed, S.W. Abdalqadir, A.R. Mohammed, *J. Mater. Sci. Mater. Electron.* **28**, 7473 (2017)
47. A. El Sayed, S. El-Sayed, W. Morsi, S. Mahrous, A. Hassen, *Polym. Compos.* **35**, 1842 (2014)
48. T. Kohoutek, J. Orava, T. Sawada, H. Fudouzi, *J. Colloid Interface Sci.* **353**, 454 (2011)
49. A. Iadicicco, S. Campopiano, D. Paladino, A. Cutolo, A. Cusano, *Opt. Express* **15**, 15011 (2007)
50. S. Wemple, M. DiDomenico Jr., *Phys. Rev. B* **3**, 1338 (1971)
51. O.G. Abdullah, Y.A. Salman, S.A. Saleem, *Phys. Mater. Chem.* **3**, 18 (2015)
52. K. Tanaka, *Thin Solid Film* **66**, 271 (1980)
53. E. Güneri, A. Kariper, *J. Alloy. Compd.* **516**, 20 (2012)
54. M. Mahdi, S. Al-Ani, *Int. J. Nanoelectron. Mater.* **5**, 11 (2012)
55. M. Frumar, J. Jedelský, B. Frumarova, T. Wagner, M. Hrdlička, *J. Non-cryst. Solids* **326**, 399 (2003)
56. R. Ahmed, A. Ibrahim, E. El-Said, *Opt. Spectrosc.* **128**, 642 (2020)
57. M. Ghanipour, D. Dorrnian, *J. Nanomater.* (2013). <https://doi.org/10.1155/2013/897043>
58. K. Aly, F.M. Abdel-Rahim, *J. Alloys Compd.* **561**, 284 (2013)
59. T. Taha, *Polym. Bull.* **76**, 903 (2019)
60. S. Sarkar, N. Das, K. Chattopadhyay, *Solid State Sci.* **33**, 58 (2014)
61. R.J. Lanzafame, *Photomed. Laser Ther.* **25**, 58 (2007)
62. M.M. Atta, E.O. Taha, A.M. Abdelreheem, *Appl. Phys. A* **127**, 532 (2021)
63. M. Bastiurea, M. Rodeanu, D. Dima, M. Murarescu, G. Andrei, *Dig. J. Nanomater. Biostruct. (DJNB)* **10**, 521–533 (2015)
64. A. Al-Sabagh, E. Taha, U. Kandil, A. Awadallah, G.M. Nasr, M. Reda Taha, *Polymers* **9**, 94 (2017)
65. C. Cai, L. Liu, Y. Fu, *Polym. Compos.* **40**, 389 (2019)

66. J. Jyoti, B.P. Singh, A.K. Arya, S. Dhakate, RSC Adv. **6**, 3997 (2016)
67. S.K. Tiwari, G. Hatui, R. Oraon, A. De Adhikari, G.C. Nayak, Curr. Appl. Phys. **17**, 1158 (2017)
68. D. Kumar, N. Kumar, P. Jindal, J. Thermoplast. Compos. Mater. (2020). <https://doi.org/10.1177/0892705720930748>
69. S.V. Kumar, K.S. Kumar, H.S. Jailani, G. Rajamurugan, Mater. Res. Express **7**, 085302 (2020)
70. J. Jyoti, A.K. Arya, Polym. Test **91**, 106839 (2020)

**Publisher's Note** Springer Nature remains neutral with regard to jurisdictional claims in published maps and institutional affiliations.